Vortex lattice effects on low-energy excitations in *d*-wave and *s*-wave superconductors

Masanori Ichioka, Akiko Hasegawa, and Kazushige Machida
Department of Physics, Okayama University, Okayama 700-8530, Japan
(Received 7 October 1998)

Generic features of the low-energy excitations in the vortex lattice state are examined by comparatively studying the self-consistent solutions of the quasiclassical Eilenberger theory both for $d_{x^2-y^2}$-wave and *s*-wave pairings. This low-energy physics associated with a vortex core, nodal structure, and quasiparticle transfer between vortices governs physical properties of the vortex such as the field dependences of the zero-energy density of states, the internal field distribution, and the shrinkage of the core radius. Eminent differences between two pairings are highlighted to help analyze experimental data. [S0163-1829(99)00102-2]

Much attention has been focused on a vortex structure in high-T_c superconductors. Many researchers try to detect the $d_{x^2-y^2}$-wave nature of the superconductivity in the vortex structure. The point is how the vortex structure is affected by the anisotropy of the energy gap in the $d_{x^2-y^2}$-wave pairing, particularly by its nodal structure. Volovik[1] theoretically suggested that the zero-energy density of states (DOS) $N(0)$ depends on a magnetic field H as $N(0)\propto\sqrt{H}$ in the $d_{x^2-y^2}$-wave pairing and $N(0)\propto H$ in the *s*-wave pairing. While a $\sqrt{H}$-like behavior was observed in specific-heat experiments,[2,3] it is uncertain whether it is exactly $\sqrt{H}$ or not. Deviations from $N(0)\propto H$ were also reported in *s*-wave superconductors.[4,5] Low-energy excitations in the vortex state can be divided conceptually into (1) those from the continuum states associated with the nodal structure, (2) the core excitations from the bound states localized in a vortex core, and (3) the quasiparticle transfer between vortices, i.e., vortex lattice effect. While Volovik's calculation takes account of only item (1), which is valid near the lower critical field H_{c1}, the other two are also indispensable when considering the low-energy physics of the vortex state in general. In order to help establish the general features of the mixed state both in $d_{x^2-y^2}$- and *s*-wave cases, one needs to calculate the vortex structure by taking into account these three contributions on an equal footing. Through these efforts we may gain a more valid and vivid picture of the vortex for whole region of $H_{c1}<H<H_{c2}$ (H_{c2} is the upper critical field).

Experimentally several important means to probe the vortex structure are now available such as muon spin resonance[6,7] (μSR) and small-angle neutron scattering (SANS) through the field distribution or by scanning tunneling microscopy[8,9] (STM) through the local density of states (LDOS) in various superconductors, including high-T_c superconductors. These data are often analyzed within conventional phenomenological theories such as Ginzburg-Landau (GL) theory or London theory. The GL theory is, strictly speaking, valid only near the transition temperature T_c. As for the London theory, which is applied near H_{c1}, the cutoff procedure of the core radius is too rough an approximation to estimate the contribution of the vortex core. In this sense it is highly needed to develop a microscopic theory in order to correctly analyze valuable experimental data. While $N(0)$ was also studied by the Brandt *et al.* theory,[5,10] it can be applied near H_{c2} since the pair potential at H_{c2} is used in the calculation.

The main purpose of this paper is to comparatively examine low-energy excitations in the vortex lattice both for $d_{x^2-y^2}$- and *s*-wave cases in order to extract the generic features of the low-energy physics of the mixed state in connection with items (1)–(3) mentioned above. Specifically we investigate various aspects of the vortex lattice structure based on the quasiclassical Eilenberger theory, which can be applied in most regions of the mixed state. We calculate the spatial variation of the order parameter, magnetic field, and LDOS in the $d_{x^2-y^2}$- and *s*-wave pairings, focusing on the difference between the two pairings. As for the single vortex case, the fourfold symmetric vortex core structure of the $d_{x^2-y^2}$-wave pairing was shown in Ref. 11. In this paper on the vortex lattice case, we can automatically include the effect of the quasiparticle transfer between vortices and study the field dependence of the vortex structure, such as $N(0)$, the core radius, or form factors of the internal field distribution.

Our calculation is performed in the clean limit after the method of Refs. 12 and 13. The Fermi surface is assumed to be cylindrical, which is appropriate to high-T_c superconductors. In our calculation, where the magnetic field is applied along the *c* axis (or *z* axis), the shape of the vortex lattice is fixed to be a square lattice tilted by 45° from the *a* axis. Some theoretical calculations suggested that this configuration of the vortex lattice has lower free energy than that of the conventional 60° triangular lattice in wide region of the higher-field and lower-temperature side in the mixed state for the $d_{x^2-y^2}$-wave pairing.[10,14,15] The STM experiment on $YBa_2Cu_3O_{7-\delta}$ (YBCO) also suggested this vortex lattice configuration in the $d_{x^2-y^2}$-wave case.[9] We calculate the vortex lattice structure of the *s*-wave pairing by using the same square lattice to clarify the effect of low-lying excitations associated with the gap anisotropy.

First, we obtain the pair potential and vector potential self-consistently by solving the Eilenberger equation in the Matsubara frequency $\omega_n=(2n+1)\pi T$. We consider the quasiclassical Green's functions $g(i\omega_n,\theta,\mathbf{r})$, $f(i\omega_n,\theta,\mathbf{r})$, and $f^{\dagger}(i\omega_n,\theta,\mathbf{r})$, where $\mathbf{r}$ is the center-of-mass coordinate of a Cooper pair. The direction of the relative momentum of the

Cooper pair, $\hat{\mathbf{k}}=\mathbf{k}/|\mathbf{k}|$, is denoted by an angle θ measured from the a axis in the ab plane. The Eilenberger equation is given by

$$\left[\omega_n+\frac{i}{2}\mathbf{v}_{\mathrm{F}}\cdot\left(\frac{\nabla}{i}+\frac{2\pi}{\phi_0}\mathbf{A}(\mathbf{r})\right)\right]f(i\omega_n,\theta,\mathbf{r})=\Delta(\theta,\mathbf{r})g(i\omega_n,\theta,\mathbf{r}),$$
$$\left[\omega_n-\frac{i}{2}\mathbf{v}_{\mathrm{F}}\cdot\left(\frac{\nabla}{i}-\frac{2\pi}{\phi_0}\mathbf{A}(\mathbf{r})\right)\right]f^{\dagger}(i\omega_n,\theta,\mathbf{r})=\Delta^{*}(\theta,\mathbf{r})g(i\omega_n,\theta,\mathbf{r}), \quad (1)$$

where $g(i\omega_n,\theta,\mathbf{r})=[1-f(i\omega_n,\theta,\mathbf{r})f^{\dagger}(i\omega_n,\theta,\mathbf{r})]^{1/2}$, $\mathrm{Re}g(i\omega_n,\theta,\mathbf{r})>0$, and $\mathbf{v}_{\mathrm{F}}=v_{\mathrm{F}}\hat{\mathbf{k}}$ is the Fermi velocity. The vector potential is written as $\mathbf{A}(\mathbf{r})=\frac{1}{2}\mathbf{H}\times\mathbf{r}+\mathbf{a}(\mathbf{r})$ in the symmetric gauge, where $\mathbf{H}=(0,0,H)$ is an external field and $\mathbf{a}(\mathbf{r})$ is related to the internal field $\mathbf{h}(\mathbf{r})=[0,0,h(\mathbf{r})]$ as $\mathbf{h}(\mathbf{r})=\nabla\times\mathbf{a}(\mathbf{r})$. As for the pair potential $\Delta(\theta,\mathbf{r})=\Delta(\mathbf{r})\phi(\theta)$, we set $\phi(\theta)=\sqrt{2}\cos 2\theta$ for the $d_{x^2-y^2}$-wave pairing and $\phi(\theta)=1$ for the s-wave pairing. The self-consistent conditions for $\Delta(\mathbf{r})$ and $\mathbf{a}(\mathbf{r})$ are given as

$$\Delta(\theta,\mathbf{r})=N_0 2\pi T\sum_{\omega_n>0}\int_0^{2\pi}\frac{d\theta'}{2\pi}V(\theta',\theta)f(i\omega_n,\theta',\mathbf{r}), \quad (2)$$

$$\nabla\times\nabla\times\mathbf{a}(\mathbf{r})=-\frac{\pi}{\kappa^2}2\pi T\sum_{\omega_n>0}\int_0^{2\pi}\frac{d\theta}{2\pi}\frac{\hat{\mathbf{k}}}{i}g(\omega_n,\theta,\mathbf{r}), \quad (3)$$

where N_0 is the density of states at the Fermi surface, $V(\theta',\theta)=\overline{V}\phi(\theta')\phi(\theta)$ the pairing interaction, $\kappa=[7\zeta(3)/72]^{1/2}(\Delta_0/T_c)\kappa_{\mathrm{BCS}}$ with Rieman's zeta function $\zeta(3)$. And κ_{BCS} is the GL parameter in the BCS theory, Δ_0 the uniform gap at $T=0$. We set the energy cutoff $\omega_c=20T_c$. In the following, energies and lengths are measured in units of Δ_0 and $\xi_0=v_{\mathrm{F}}/\Delta_0=\pi\xi_{\mathrm{BCS}}$ (ξ_{BCS} is the BCS coherence length), respectively.

By solving Eq. (1) in the so-called explosion method[12,13] under $\Delta(\mathbf{r})$ and $\mathbf{a}(\mathbf{r})$ of the vortex lattice case, we evaluate the quasiclassical Green's functions at 40×40 discretized points in a unit cell of the vortex lattice. We obtain new $\Delta(\mathbf{r})$ and $\mathbf{a}(\mathbf{r})$ from Eqs. (2) and (3), and use them at the next step calculation of Eq. (1). This iteration procedure is repeated until a sufficiently self-consistent solution is obtained. We use the material parameters appropriate to YBCO, i.e., $\xi_{\mathrm{BCS}}=16$Å and $\kappa_{\mathrm{BCS}}=100$. Then, $H_{c2}=66.7$ T in the s-wave pairing and 93.2 T in the $d_{x^2-y^2}$-wave pairing for $T/T_c=0.5$.[16] To study the field dependence, the calculations of $\Delta(\mathbf{r})$ and $\mathbf{a}(\mathbf{r})$ are done for various fields at fixed temperature $T/T_c=0.5$. The spatial variation of current and internal fields is calculated from $\mathbf{a}(\mathbf{r})$.

Next, we calculate the LDOS for energy E as $N(E,\mathbf{r})=N_0\int_0^{2\pi}(d\theta/2\pi)\mathrm{Re}g(i\omega_n\rightarrow E+i\eta,\theta,\mathbf{r})$. Typically, we choose $\eta=0.03$. To obtain $g(i\omega_n\rightarrow E+i\eta,\theta,\mathbf{r})$, we solve Eq. (1) for $\eta-iE$ instead of ω_n using the self-consistently obtained $\Delta(\mathbf{r})$ and $\mathbf{a}(\mathbf{r})$. The zero-energy DOS, $N(0)$, is the spatial average of $N(E=0,\mathbf{r})$. We confirm that the following results are not changed qualitatively for smaller η.

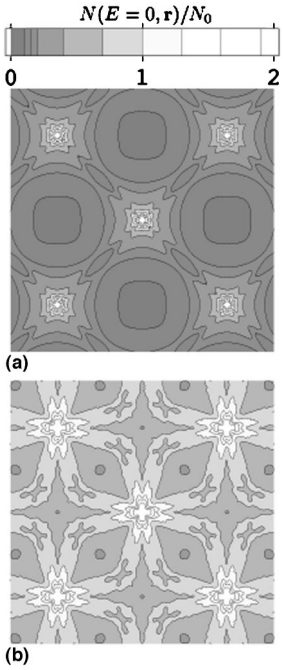

FIG. 1. Spatial variation of the LDOS for $E=0$ in the $d_{x^2-y^2}$-wave pairing. Contour plot of $N(E=0,\mathbf{r})/N_0$ is presented. (a) At low field $H/H_{c2}=0.021$. The region $14\xi_0\times 14\xi_0$ is shown. To clearly show the ridge structure, the contour lines are densely plotted for small value of LDOS. (b) At high field $H/H_{c2}=0.54$. The region $2.8\xi_0\times 2.8\xi_0$ is shown. The a axis and b axis are along the horizontal and vertical directions. There is a vortex center at each white area.

We start by discussing the spatial structure of the zero-energy LDOS $N(E=0,\mathbf{r})$, which may be directly observed by the STM experiments. In the s-wave pairing at lower fields, $N(E=0,\mathbf{r})$ is localized circularly in a small region around each vortex core, as in the single vortex case. Since the intervortex distance decreases with increasing H, the vortex lattice effect appears in $N(E=0,\mathbf{r})$ at higher fields, as reported in Ref. 12. There, $N(E=0,\mathbf{r})$ is suppressed along the lines connecting two nearest-neighbor vortex centers.

These features are contrasted with those of the $d_{x^2-y^2}$-wave pairing. In the single vortex case, as shown in Fig. 8(d) of Ref. 11, $N(E=0,\mathbf{r})$ consists of the vortex core contribution and four eminent tails extended from the vortex center along lines of the node direction ($\theta=\pi/4$ and its equivalent directions). Strictly speaking, this low-energy state is not a bound state as the tails extend toward infinite points.[17] These tails arisen from the nodal structure of the $d_{x^2-y^2}$-wave pairing can be seen in our calculation of the vortex lattice case at low field [Fig. 1(a) for $H=0.021H_{c2}$]. It is noted, however, that each tail slightly splits into two ridges between vortices. This split is due to the vortex lattice effect, i.e., the suppression along the line between nearest-neighbor vortex centers. The vortex lattice effect appears even from the lower fields in the $d_{x^2-y^2}$-wave pairing. It means that the quasiparticle transfer between vortices is large in the $d_{x^2-y^2}$-wave case due to the tail structure of $N(E=0,\mathbf{r})$. The split is enhanced on raising the field, as shown in Fig. 1(b) for $H=0.54H_{c2}$. Therefore, the tail struc-

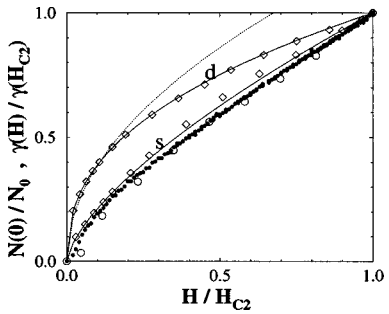

FIG. 2. Field dependence of $N(0)/N_0$ in the $d_{x^2-y^2}$- and s-wave pairings ($\diamond$). Solid and dotted lines are fitting lines. Experimental data $\gamma(H)/\gamma(H_{c2})$ are also plotted for $CeRu_2$ ($\bullet$) (Ref. 5) and $NbSe_2$ ($\circ$) (Ref. 19).

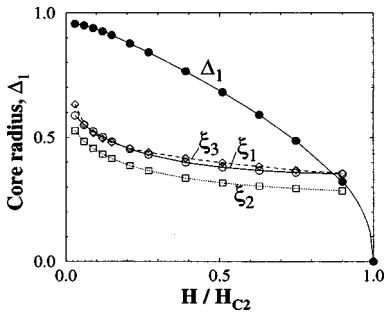

FIG. 3. Field dependence of core radius ξ_1, ξ_2, and ξ_3 for the s-wave pairing. Maximum amplitude of the order parameter Δ_1 is also plotted. The radius and Δ_1 are, respectively, scaled by ξ_0 and Δ_0. Lines are guides for the eye.

ture along the node directions in $N(E=0,\mathbf{r})$ is smeared by the vortex lattice effect at higher field, where the tails extend toward rather different directions. This may be a possible reason why we do not clearly detect the four tails of the node direction around a vortex in the STM experiment on YBCO.[9]

Let us analyze the field dependence of $N(0)$ in view of the above structure of low-energy excitations around a core for the $d_{x^2-y^2}$- and s-wave pairings. According to Volovik[1] for the $d_{x^2-y^2}$-wave case, the contribution to $N(0)$ mainly comes from the tail structure along the node direction in $N(E=0,\mathbf{r})$. The length of the tail is the order of $H^{-1/2}$ (lattice constant of the vortex lattice). As the vortex density is proportional to H, $N(0)$ is roughly estimated as $N(0) \sim H^{-1/2}H=\sqrt{H}$. This estimate becomes uncertain at higher field, since the tail structure along the node directions is smeared by the vortex lattice effect as shown in Fig. 1. We present our result for the field dependence of $N(0)$ in Fig. 2. The difference between the $d_{x^2-y^2}$ and s waves is clearly seen, where the latter has no tail structure in $N(E=0,\mathbf{r})$. However, the dependence in the $d_{x^2-y^2}$-wave pairing deviates from $\sqrt{H}$ behavior (the curve for $\sqrt{H}$ is plotted by dotted line).[18] The best fit is obtained by $N(0)/N_0=(H/H_{c2})^{0.41}$ (solid line). Its exponent 0.41 is slightly smaller than 0.5 of the Volovik theory. Experimentally, $N(0)$ is obtained from the coefficient of the T-linear term in the specific heat $C(T)$, i.e., $N(0)\propto\gamma(H)=\lim_{T\to 0}C(T)/T$. So far, the $\sqrt{H}$ behavior of $\gamma(H)$ was examined within the low-field region.[2,3] The deviation from $\sqrt{H}$ is expected when $\gamma(H)$ is measured in higher-field regions.

As for the s-wave pairing case, our data in Fig. 2 also deviate from a naively expected relation that $N(0)$ is proportional to the vortex density, i.e., $N(0)\propto H$. The best fit is obtained by $N(0)/N_0=(H/H_{c2})^{0.67}$ (solid line). In Fig. 2, we also plot the field dependence of $\gamma(H)/\gamma(H_{c2})$, which corresponds to $N(0)/N_0$, for $CeRu_2$ (Ref. 5) and $NbSe_2$ (Ref. 19). These experimental data for typical s-wave superconductors apparently deviate from H-linear behavior and fit with a similar curve to our calculation of the s-wave pairing. We note that the borocarbide superconductor $LuNi_2B_2C$ shows $\sqrt{H}$-like behavior of $\gamma(H)$,[4] that is, d-wave-like behavior of Fig. 2. While it is considered to be an s-wave superconductor, it has a highly anisotropic Fermi surface with fourfold symmetry.[15,20] Then, $\sqrt{H}$-like behavior may occur due to the Fermi-surface anisotropy instead of the gap anisotropy, both of which give rise to a similar effect on $N(0)$ in the result.

To understand the origin of the deviation from H-liner behavior in the s-wave pairing, we show the field dependence of the vortex core radius in Fig. 3. The radius ξ_1 is defined from the initial slope of the pair potential by fitting as $|\Delta(\mathbf{r})|=\Delta_1 r/\xi_1$ at the vortex center. There, Δ_1 is defined as the maximum of $|\Delta(\mathbf{r})|$ along the line connecting the nearest-neighbor vortex centers. The radius ξ_2 is defined as the one where the screening current around a vortex has its maximum. When increasing H, both ξ_1 and ξ_2 decrease similarly as seen in Fig. 3. The $d_{x^2-y^2}$-wave case shows the similar decrease about the core radius. The shrinkage of the core radius was also reported by the experiments of STM (Ref. 8) and μSR (Ref. 6). In the calculation of a single vortex,[21] zero-energy DOS per vortex $N(0)/H$ is proportional to an area of the vortex core $\pi\xi_3^2$. In Ref. 21, the radius ξ_3 corresponds to our ξ_1. If ξ_3 is independent of H, we obtain the naively expected relation $N(0)\propto H$. However, it is not the case. In Fig. 3, we also plot the core radius ξ_3 estimated from $N(0)$, where $\xi_3=0.35[(N(0)/N_0)/(H/H_{c2})]^{1/2}$ with a fitting parameter 0.35. The radius ξ_3 decreases similarly as ξ_1 with increasing H. It means that the deviation from H linear in $N(0)$ does reflect the field dependence of the core radius.

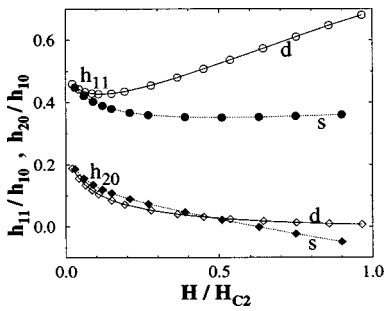

FIG. 4. Field dependence of form factors. For the $d_{x^2-y^2}$- and s-wave pairings, $h_{1,1}/h_{1,0}$ and $h_{2,0}/h_{1,0}$ are plotted. Lines are guides for the eye. For the $d_{x^2-y^2}$-wave pairing, $h_{1,1}/h_{1,0}$ increases with approaching H_{c2}, and $h_{2,0}/h_{1,0}$ remains positive and approaches 0 for $H\to H_{c2}$. For the s-wave pairing, $h_{1,1}/h_{1,0}$ remains almost constant at higher field, and $h_{2,0}/h_{1,0}$ becomes negative for $H\to H_{c2}$.

Lastly, we study the difference between $d_{x^2-y^2}$- and s-wave pairings in the internal field $h(\mathbf{r})$. The spatial variation of $h(\mathbf{r})$ is characterized by the form factor $h_{m,n}$ (m,n are integer). It is the Fourier component of $h(\mathbf{r})$ defined as $h(\mathbf{r})=H\Sigma_{m,n}h_{m,n}\exp(i\mathbf{g}_{m,n}\cdot\mathbf{r})$ with reciprocal lattice vector $\mathbf{g}_{m,n}=-n\mathbf{k}_1+m\mathbf{k}_2$. The spatial variation of $h(\mathbf{r})$ shows fourfold symmetry around a vortex core in the $d_{x^2-y^2}$-wave pairing, while it is circular in the s-wave pairing.[11] This difference becomes clear at higher field, and reflects the field dependence of $h_{1,1}$ and $h_{2,0}$ as shown in Fig. 4. We note that clear difference does not appear in $h_{1,0}$, $h_{2,1}$, and $h_{3,0}$. These differences can be detected by SANS, and may appear also in the resonance line shape in the μSR. We confirm that the results of Fig. 4 are not changed qualitatively in the triangular lattice case.

In summary, we have extracted the generic features of low-energy excitations in the vortex lattice both for $d_{x^2-y^2}$- and s-wave pairings by solving the quasiclassical Eilenberger theory. The three low-energy features are (1) from the continuum state associated with the nodal structure, (2) the core excitations from the bound states, and (3) the quasiparticle transfer between vortices as identified and examined by emphasizing the importance upon the vortex physics. These features give rise to the clear difference between $d_{x^2-y^2}$- and s-wave pairings in the field dependence of $N(0)$ and the form factors $h_{1,1}$ and $h_{2,0}$. The vortex lattice effect gives the deviation from $\sqrt{H}$ behavior of $N(0)$ in the $d_{x^2-y^2}$-wave pairing. As the vortex core radius decreases with increasing field, $N(0)$ deviates from H-linear behavior in the s-wave pairing. The contribution of vortex core region and the vortex lattice effect (i.e., the quasiparticle transfer between vortices) are also important when we experimentally and theoretically investigate the detailed structure of the vortex state.

[1] G. E. Volovik, Pis'ma Zh. Eksp. Teor. Fiz. **58**, 457 (1993) [JETP Lett. **58**, 469 (1993)].
[2] K. A. Moler *et al.*, Phys. Rev. Lett. **73**, 2744 (1994).
[3] R. A. Fisher *et al.*, Physica C **252**, 237 (1995).
[4] M. Nohara *et al.*, J. Phys. Soc. Jpn. **66**, 1888 (1997).
[5] M. Hedo *et al.*, J. Phys. Soc. Jpn. **67**, 33 (1998).
[6] J. Sonier *et al.*, Phys. Rev. Lett. **79**, 1742 (1997).
[7] J. Sonier *et al.*, Phys. Rev. Lett. **79**, 2875 (1997).
[8] A. A. Golubov and U. Hartmann, Phys. Rev. Lett. **72**, 3602 (1994).
[9] I. Maggio-Aprile *et al.*, Phys. Rev. Lett. **75**, 2754 (1995); J. Low Temp. Phys. **105**, 1129 (1996).
[10] H. Won and K. Maki, Phys. Rev. B **53**, 5927 (1996).
[11] M. Ichioka, N. Hayashi, N. Enomoto, and K. Machida, Phys. Rev. B **53**, 15 316 (1996).
[12] M. Ichioka, N. Hayashi, and K. Machida, Phys. Rev. B **55**, 6565 (1997).
[13] U. Klein, J. Low Temp. Phys. **69**, 1 (1987); , Phys. Rev. B **40**, 6601 (1989); B. Pöttinger and U. Klein, Phys. Rev. Lett. **70**, 2806 (1993).
[14] M. Ichioka, N. Enomoto, and K. Machida, J. Phys. Soc. Jpn. **66**, 204 (1997).
[15] Y. De Wilde *et al.*, Phys. Rev. Lett. **78**, 4273 (1997). Their calculation of the GL theory can be applied to the $d_{x^2-y^2}$-wave case.
[16] T. Sugiyama (private communication).
[17] M. Franz and Z. Tešanović, Phys. Rev. Lett. **80**, 4763 (1998).
[18] Y. Wang and A. H. MacDonald, Phys. Rev. B **52**, 3876 (1995). Similar deviation is reported by the Bogoliubov–de Gennes theory for the extended Hubbard model.
[19] M. Nohara (private communication). Also see Ref. 4.
[20] V. Metlushko *et al.*, Phys. Rev. Lett. **79**, 1738 (1997).
[21] A. L. Fetter and P. C. Hohenberg, in *Superconductivity*, edited by R. D. Parks (Marcel Dekker, New York, 1969), p. 891.